Simulation of the energy distribution of relativistic electron precipitation caused by quasi-linear interactions with EMIC waves

Zan Li,[1] Robyn M. Millan,[1] and Mary K. Hudson[1]

Received 2 August 2013; revised 10 November 2013; accepted 12 November 2013; published 5 December 2013.

[1] Previous studies on electromagnetic ion cyclotron (EMIC) waves as a possible cause of relativistic electron precipitation (REP) mainly focus on the time evolution of the trapped electron flux. However, directly measured by balloons and many satellites is the precipitating flux as well as its dependence on both time and energy. Therefore, to better understand whether pitch angle scattering by EMIC waves is an important radiation belt electron loss mechanism and whether quasi-linear theory is a sufficient theoretical treatment, we simulate the quasi-linear wave-particle interactions for a range of parameters and generate energy spectra, laying the foundation for modeling specific events that can be compared with balloon and spacecraft observations. We show that the REP energy spectrum has a peaked structure, with a lower cutoff at the minimum resonant energy. The peak moves with time toward higher energies and the spectrum flattens. The precipitating flux, on the other hand, first rapidly increases and then gradually decreases. We also show that increasing wave frequency can lead to the occurrence of a second peak. In both single- and double-peak cases, increasing wave frequency, cold plasma density or decreasing background magnetic field strength lowers the energies of the peak(s) and causes the precipitation to increase at low energies and decrease at high energies at the start of the precipitation.

Citation: Li, Z., R. M. Millan, and M. K. Hudson (2013), Simulation of the energy distribution of relativistic electron precipitation caused by quasi-linear interactions with EMIC waves, *J. Geophys. Res. Space Physics*, *118*, 7576–7583, doi:10.1002/2013JA019163.

1. Introduction

[2] The flux of radiation belt electrons is highly variable, especially during geomagnetic storms. However, the role played by each of several acceleration and loss mechanisms is not yet established observationally [*Millan and Thorne*, 2007]. Precipitation into the atmosphere is considered to be one of the major electron loss mechanisms, which can completely deplete the radiation belts of electrons during the main phase of some geomagnetic storms [*O'Brien et al.*, 2004; *Selesnick*, 2006]. Using data from balloon-borne X-ray detectors, *Foat et al.* [1998], *Lorentzen et al.* [2000], and *Millan et al.* [2002] have reported precipitating relativistic electrons in the dusk sector. These duskside precipitation events occur over a variety of magnetic activity levels [*Lorentzen et al.*, 2000; *Kokorowski et al.*, 2008] and a broad radial distribution ranging from L = 3–8 [*Millan et al.*, 2013]. The energy spectrum has been found to be well fit by an exponential distribution with an e-folding energy ranging from 0.5 to 3.6 MeV [*Millan et al.*, 2002].

[3] Based primarily on the fact that all these events were found at dusk, the cause has been suggested to be the gyroresonant scattering by electromagnetic ion cyclotron (EMIC) waves. EMIC waves are observed throughout the inner magnetosphere but predominantly on the duskside and dayside [*Anderson et al.*, 1992a, 1992b; *Meredith*, 2003; *Erlandson and Ukhorskiy*, 2001; *Fraser et al.*, 1996, 2006; *Usanova et al.*, 2012]. They are excited by anisotropic ring current ions injected into the inner magnetosphere [e.g., *Jordanova et al.*, 2008] or by compressions of the magnetopause [e.g., *Anderson and Hamilton*, 1993]. The linear growth rate of EMIC waves maximizes in high-density regions such as the duskside plasmapause or plasmaspheric drainage plume due to reduced resonant energies [*Cornwall et al.*, 1970; *Horne and Thorne*, 1993] and wave guiding by steep density gradients near the plasmapause [*Horne and Thorne*, 1993; *Jordanova et al.*, 2001; *Chen et al.*, 2009]. Field-aligned EMIC waves interact with relativistic electrons through the gyroresonance condition

$$\omega - k_{\|} v_{\|} = -|\Omega_e|/\gamma \tag{1}$$

[1]Department of Physics and Astronomy, Dartmouth College, Hanover, New Hampshire, USA.

Corresponding author: Z. Li, Department of Physics and Astronomy, 6127 Wilder Lab, Dartmouth College, Hanover, NH 03755, USA. (Zan.Li.GR@dartmouth.edu)

2169-9380/13/10.1002/2013JA019163

where Ω_e is electron gyrofrequency, γ is the relativistic factor, $k_{\|}$ and $v_{\|}$ are components of the wave propagation vector and particle velocity along the direction of the ambient magnetic field. EMIC waves are expected to effectively scatter relativistic electrons of geophysically interesting energies, preferably in duskside high-density regions, where the minimum energy limit is relatively low and the diffusion rate is close to the strong diffusion limit [*Thorne and Kennel*, 1971; *Albert*, 2003; *Summers*, 2003]. Duskside simultaneous proton and relativistic electron precipitation has also been observed, supporting the theory of precipitation caused by EMIC wave scattering [e.g., *Bortnik et al.*, 2006]. Several wave-particle interaction models have been proposed. Quasi-linear theory [*Kennel and Petschek*, 1966] has been the dominant treatment; however, recent work shows that nonlinear effects can be very significant and even reverse the conclusions [*Albert and Bortnik*, 2009]. Therefore, it is important to establish when and where each approach is applicable and to test these models with observations.

[4] Existing theoretical discussions on EMIC waves as a possible loss mechanism mainly focus on the evolution of the trapped electron flux and its timescale. However, directly measured by balloon detectors is the energy spectrum of the bremsstrahlung X-rays produced by the precipitating electrons, and many satellites also measure the energy of the precipitating electrons [*Millan et al.*, 2007]. It is very important to understand the energy dependence of the precipitating flux driven by EMIC waves, as well as the time evolution of this dependence in order to test the theory with observations. This paper uses the quasi-linear formulation to evaluate the energy and time dependence of REP, and investigates how different parameters affect the diffusion coefficients and the energy spectrum. When applied with input wave and particle data from satellites (e.g., Van Allen Probes, GOES), the results from our model can be directly compared with balloon (e.g., Balloon Array for RBSP (Radiation Belt Storm Probes) Relativistic Electron Losses) and low-altitude satellite (e.g., Solar Anomalous and Magnetospheric Particle Explorer (SAMPEX) and Polar-orbiting Operational Environmental Satellites (POES)) measurements to investigate the role of EMIC waves in causing REP as well as the effectiveness of the adopted theoretical model.

2. Diffusion Equation

[5] We use quasi-linear diffusion theory to model the evolution of the distribution of electrons due to interactions with EMIC waves. Radial and energy diffusion are ignorable because the frequency of the EMIC waves is well above the drift frequency and well below the gyrofrequency of the resonant particles [*Kennel*, 1966]. The bounce-averaged diffusion equation for pure pitch angle scattering can be written as [*Davidson and Walt*, 1977; *Lyons*, 1973; *Lyons and Williams*, 1984; *Shao et al.*, 2009]

$$\frac{\partial f_0}{\partial t} = \frac{1}{\sin(2\alpha_0)T(\alpha_0)}\frac{\partial}{\partial \alpha_0}\left(\sin(2\alpha_0)T(\alpha_0)\langle D_{\alpha\alpha}(\alpha_0,E)\rangle\frac{\partial f_0}{\partial \alpha_0}\right) - \frac{f_0}{\tau_{\text{atm}}} \quad (2)$$

where $T(\alpha_0) = 1.3802 - 0.3198\left(\sin(\alpha_0) + \sin^{1/2}(\alpha_0)\right)$ is the normalized bounce time, f_0 is the trapped electron phase space density, α_0 is the equatorial pitch angle, $\langle D_{\alpha\alpha}(\alpha_0, E)\rangle$ is the bounce-averaged pitch angle diffusion coefficient, and τ_{atm} is the timescale for losses to the atmosphere. Assuming that losses occur only from within the loss cone and that the loss cone is emptied twice per bounce period, we take τ_{atm} to be half of the bounce period inside the loss cone and infinite outside the loss cone [*Lyons*, 1973; *Davidson and Walt*, 1977; *Lyons and Williams*, 1984; *Shao et al.*, 2009]. The differential flux is related to the phase space density through the electron momentum p as $j_0 = p^2 f_0$. To capture the feature of the isotropic flux distribution in the loss cone in the many strong diffusion cases in our parameter studies, we set the boundary conditions to be $\frac{\partial j_0}{\partial \alpha_0}|_{\alpha_0=0^o} = \frac{\partial j_0}{\partial \alpha_0}|_{\alpha_0=90^o} = 0$. For weak diffusion cases, although $\frac{\partial j_0}{\partial \alpha_0}|_{\alpha_0=0^o}$ does not have to be zero, the loss cone is essentially empty and a small number of electrons in the loss cone does not significantly affect the diffusion [*Shprits et al.*, 2009]. The initial flux is chosen to be [*Tao et al.*, 2009]

$$j_0(t=0) = [\sin(\alpha_0) - \sin(\alpha_{0L})]\exp[-(E-0.2)/0.1] \quad (3)$$

with an arbitrary scaling outside the loss cone and $j_0(t = 0) = 0$ inside the loss cone. Here E is the particle energy in MeV and α_{0L} is the equatorial loss cone angle given by $\sin^2(\alpha_{0L}) = (4L^6 - 3L^5)^{-1/2}$ at a particular L shell.

3. Diffusion Coefficients

[6] We calculate the bounce-averaged diffusion coefficient using the same method as *Summers* [2003] and *Summers et al*. [2007] for parallel-propagating EMIC waves in a multi-ion (H^+, He^+, and O^+) plasma. The diffusion coefficient is corrected with a factor of 2 [*Albert*, 2007]. The Earth's magnetic field is assumed dipolar, the wave amplitude is taken to be 1 nT, and the wave frequency spectrum is assumed to be a truncated Gaussian, namely,

$$\tilde{W}(\omega) \propto \exp\{-[(\omega-\omega_m)/\delta\omega]^2\} \quad (4)$$

where ω_m is the center frequency, with lower frequency limit $\omega_1 = \omega_m - \delta\omega$ and upper frequency limit $\omega_2 = \omega_m + \delta\omega$. $\delta\omega$ is a measure of the bandwidth. The EMIC waves are assumed to be confined to $\pm 15\%$ in latitude and 10% of the electron drift orbit, propagating in a cold plasma of a storm time ion composition 70% H^+, 20% He^+, and 10% O^+ [*Meredith*, 2003]. The wave dispersion relation is

$$\frac{c^2k^2}{\omega^2} = 1 - \frac{\omega_{pe}^2}{\omega(\omega+|\Omega_e|)} - \sum_{j=1}^{3}\frac{\omega_{pj}^2}{\omega(\omega-\Omega_j)} \quad (5)$$

where k is the wave number $k_1 < k < k_2$. The suffix j denotes the ion species; the values $j = 1, 2,$ and 3 refer to H^+, He^+, and O^+, respectively. The minimum resonant energy can be approximated as [*Summers*, 2003]

$$E_{\min} \sim (1 + \frac{\Omega_e^2}{c^2k_2^2})^{1/2} - 1 \quad (6)$$

[7] Figure 1 shows the bounce-averaged diffusion coefficient as a function of equatorial pitch angles we calculated for 0.1–5 MeV electrons with four sets of equatorial

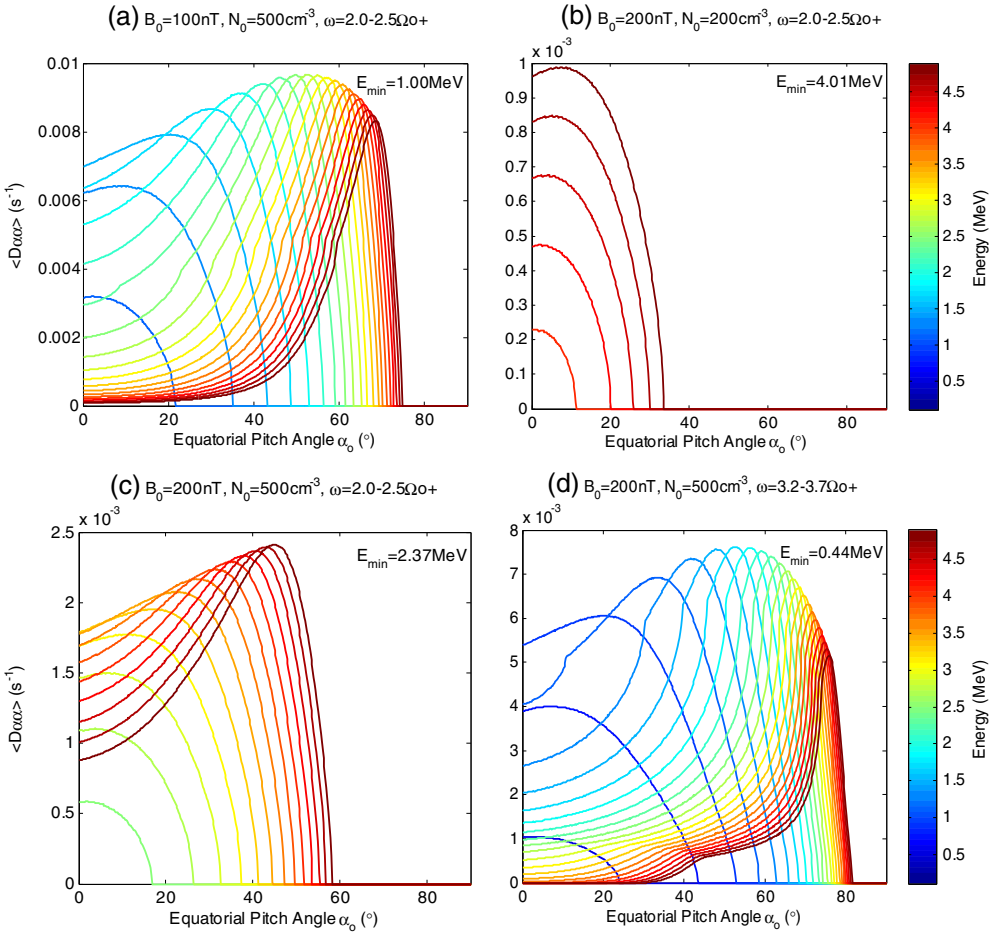

Figure 1. Bounce-averaged pitch angle diffusion coefficients for EMIC waves interacting with electrons of energies 0.1–5 MeV with an increment of 0.2 MeV and four different sets of wave and plasma parameters. Minimum resonant energies are indicated in the upper right corner of each graph.

background magnetic field strength B_0, cold plasma density N_0, and wave frequency ω. Each diffusion coefficient spans from 0° to an upper resonant pitch angle limit α_{0u} and maximizes to a value $\langle D_{\alpha\alpha}(\alpha_0, E)\rangle_m$ at a pitch angle α_{0m}.

[8] We next investigate how the diffusion coefficient varies with energy and pitch angles for a full range of parameters B_0, N_0, and ω. The varying diffusion coefficients will determine how the energy spectrum evolves (section 4). We choose B_0, N_0, and ω to vary from 75 to 1150 nT (corresponding to $L \sim$ 3–8), 1 to 1000 cm^{-3} (assumed to be constant over the entire interaction region), and 1.9 to 3.9 Ω_{O+} (covering roughly the entire helium band, where the spectral intensity of EMIC waves is enhanced [*Thorne et al.*, 2006; *Anderson et al.*, 1992a; *Hu et al.*, 2010] and pitch angle diffusion of geophysically interesting relativistic electrons is more likely to occur [*Li et al.*, 2007]), respectively. Since EMIC waves are often observed near the geosynchronous orbit where $N_0 \lesssim 100$ cm^{-3} [*Halford et al.*, 2010], we set the control B_0 and N_0 to be 100 nT and 100 cm^{-3}, respectively. We also choose the control wave frequency to be ω = 2.4–3.4 Ω_{O+}, estimated from wave observations [*Meredith*, 2003; *Ukhorskiy et al.*, 2010]. In Figure 2 (first to fourth rows) (the fifth row will be discussed in section 4), we plot $\langle D_{\alpha\alpha}(\alpha_0 \sim 0°, E)\rangle$, $\langle D_{\alpha\alpha}(\alpha_0, E)\rangle_m$, α_{0m}, and α_{0u} as a function of E to characterize the diffusion coefficient when one parameter is varied while the others are held fixed. Satisfying the gyroresonance condition equation (1), the dispersion relation equation (5), and the Gaussian wave frequency distribution equation (4), the plots show that for all B_0, N_0, ω_1, and ω_2, the pitch angles α_{0u} and α_{0m} increase monotonically with energy, whereas $\langle D_{\alpha\alpha}(\alpha_0 \sim 0°, E)\rangle$ and $\langle D_{\alpha\alpha}(\alpha_0, E)\rangle_m$ increase from the minimum resonant energy up to a certain "peak" energy and then decrease. The value of the peak energy decreases with decreasing B_0 or increasing N_0, ω_1, or ω_2. The width of the peak significantly narrows with increasing ω_1 and ω_2, meaning that at high frequencies, the diffusion coefficient sharply increases at the peak energy from surrounding energies. Keeping energy fixed, as B_0 decreases or N_0, ω_1, or ω_2 increases, α_{0m} increases monotonically; the diffusion coefficient increases at low energies yet decreases at high energies (variations at >5 MeV are not shown in the figure); $\langle D_{\alpha\alpha}(\alpha_0, E)\rangle_m$ increases at low energies and decreases at high energies only with increasing ω_2 while increases at low energies and approaches the same values at high energies with decreasing B_0 or increasing N_0 or ω_1 (variations at >5 MeV are not shown in the figure). Lastly, the minimum resonant energy $E_{\min}$ decreases while α_{0u} increases with decreasing B_0 or increasing N_0 or ω_2, but $E_{\min}$ and α_{0u} are unaffected by ω_1.

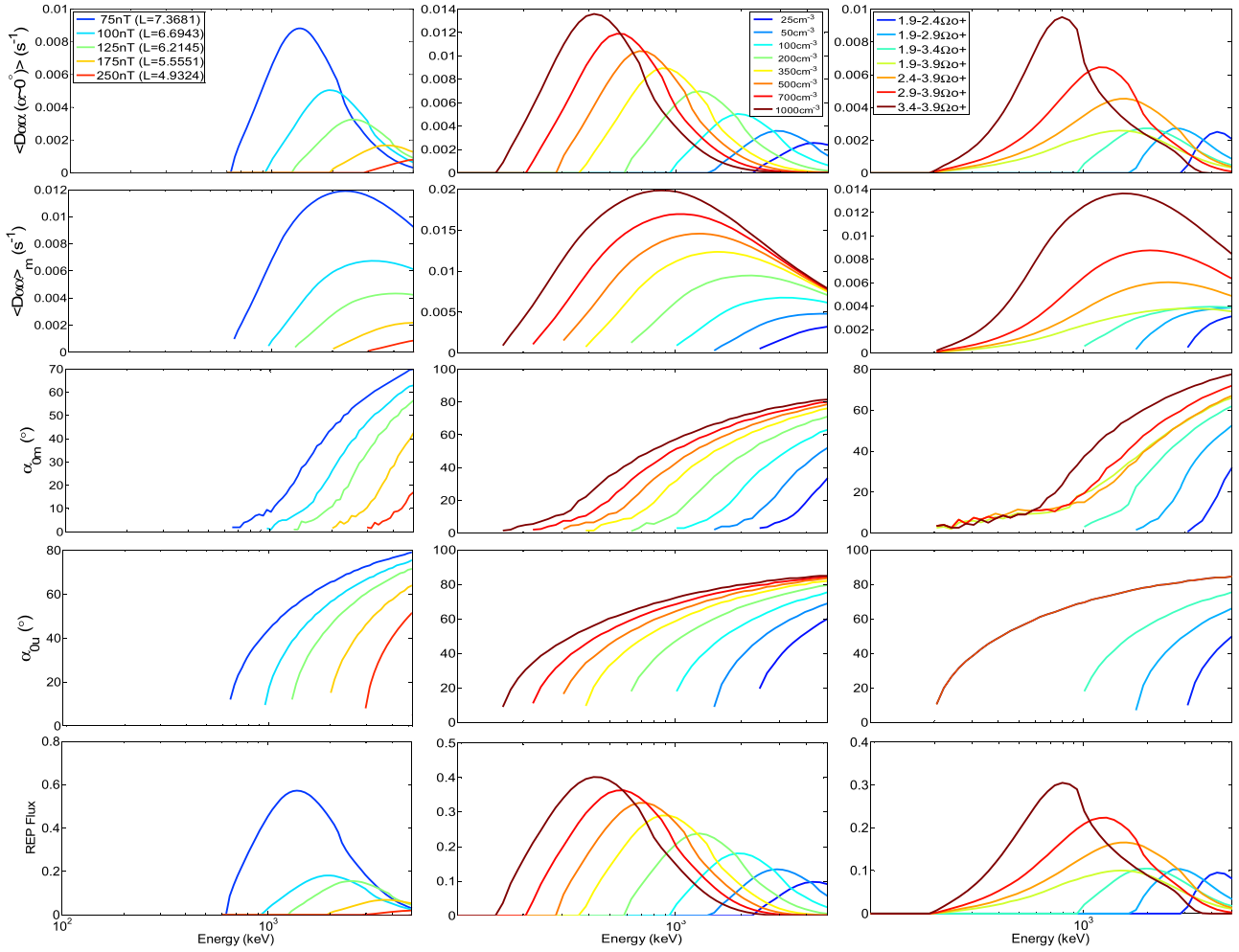

Figure 2. (first to fourth rows) $\langle D_{\alpha\alpha}(\alpha_0 \sim 0°, E)\rangle$, $\langle D_{\alpha\alpha}(\alpha_0, E)\rangle_m$, α_{0m}, and α_{0u} are shown, respectively. (fifth row) Precipitating flux at t = 1 s derived from initial distribution equation (9). Curves with minimum resonant energies above 5 MeV do not appear in the plots. (left column) Varying B_0, N_0 = 100 cm^{-3}, ω_1 = 2.4 Ω_{O+}, ω_2 = 3.4 Ω_{O+}; (middle column) varying N_0, B_0 = 100 nT, ω_1 = 2.4 Ω_{O+}, ω_2 = 3.4 Ω_{O+}; and (right column) varying ω, B_0 = 100 nT, N_0 = 100 cm^{-3} are shown. (third row, left column) The curves of the same ω_2 overlap.

4. Time Evolution of Trapped and Precipitating Electron Fluxes

[9] Applying the results for the diffusion coefficients from section 3, we solve equation (2) for the trapped equatorial electron flux $j_0(\alpha_0, E, t)$. An example is shown in Figure 3. As we can see, the loss cone fills up quickly (e.g., the first ~60 s in Figure 3) before gradually being depleted as the total flux drops due to loss to the loss cone.

[10] The omnidirectional flux at any latitude λ on a dipole field line can be expressed in terms of equatorial flux and pitch angles as [*Lyons and Williams*, 1984],

$$J_\lambda(E,t) = \frac{4\pi B_\lambda}{B_0}\int_0^{\alpha^\star} j_0(\alpha_0,E,t)\frac{(1-\sin^2\alpha_0)^{1/2}}{(1-\frac{B_\lambda}{B_0}\sin^2\alpha_0)^{1/2}}\sin\alpha_0 d\alpha_0 \quad (7)$$

where $\alpha^\star = \arcsin\sqrt{\frac{B_0}{B_\lambda}}$.

[11] If we take λ to be the latitude where the field line intersects the atmosphere boundary, then $B_\lambda/B_0 = (4L^6 - 3L^5)^{1/2}$, $\alpha^\star = \alpha_{0LC}$ and no particle bounces back to the equator. The omnidirectional relativistic electron precipitation (REP) flux measured at the atmosphere boundary will then be

$$J_{\mathrm{REP}}(E,t) = 2\pi(4L^6-3L^5)^{1/2} \cdot \int_0^{\alpha_{0LC}} j_0(\alpha_0,E,t)\frac{(1-\sin^2\alpha_0)^{1/2}}{[1-(4L^6-3L^5)^{1/2}\sin^2\alpha_0]^{1/2}}\sin\alpha_0 d\alpha_0 \quad (8)$$

J_{REP} plotted versus E is then the energy spectrum of the precipitating electrons.

[12] To study how the $J_{\mathrm{REP}}(E,t)$ energy spectra are affected by the diffusion coefficients, we first apply an energy-independent initial distribution

$$j_0(t=0) = \sin(\alpha_0) - \sin(\alpha_{0L}) \quad (9)$$

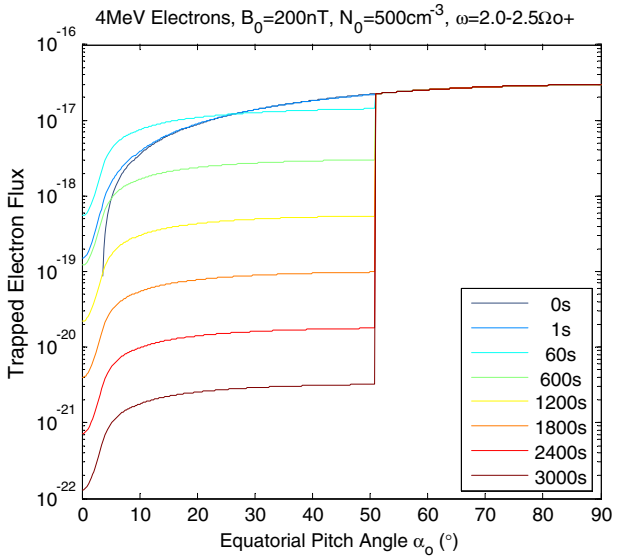

Figure 3. Evolution of the pitch angle distribution of the trapped flux of 4 MeV electrons in the simulation time 0 to 5 min. B_0, N_0, ω_1, and ω_2 are the same as Figure 1 (c). At B_0 = 200 nT ($L \sim 6.7$), the loss cone is ∼2.3°. At 0 min, the trapped flux distribution is the initial Maxwellian flux distribution equation (3).

and examine the precipitation spectrum in the first second, i.e., $J_{\mathrm{REP}}(E, t = 1\,\mathrm{s})$ (Figure 2, fifth row). These plots strongly resemble those of $\langle D_{\alpha\alpha}(\alpha_0 \sim 0°, E)\rangle$ (Figure 2, first row), indicating that the precipitation at the outset is largely controlled by the diffusion coefficients at small pitch angles.

[13] Next, we again use the Maxwellian initial distribution equation (3) and study how the spectrum is affected by time. We found two types of spectra (Figure 4): In most cases, the spectrum is singly peaked (Figure 4a), but occasionally, increasing wave frequency can induce another peak (Figure 4b). As shown in the figures, initially, both spectra resemble Maxwellian distributions with a lower cutoff at the minimum resonant energy. The precipitation quickly builds up from zero within the first second as the loss cone is being filled. Shortly after, the REP flux near the minimum resonant energies largely drops and the REP flux starts to gradually decrease as the loss cone is being depleted. This rapid increase and slow decrease of the precipitation is consistent with many balloon observations [*Millan et al.*, 2007]. However, in Figure 4a, the peak of the REP flux keeps moving toward higher energies and the curves flatten out. In Figure 4b, the peak stays at a roughly constant energy, followed by another peak forming at a later time at a higher energy and moving toward even higher energies. The hardening of both spectra with time is due to the fact that (1) with increasing energy, diffusion becomes increasingly dominated by particles with larger pitch angles (α_{0m} and α_{0u} both increase with energy) and they are scattered into the loss cone more slowly than the ones with smaller pitch angles; (2) over time, with fewer particles left to interact with the waves, the precipitation is largely reduced at lower energies associated with shorter lifetimes (larger diffusion coefficients) and therefore the spectrum becomes harder and more isotropic (flatter) in energy. Furthermore, as we discussed in the previous section, the increase of the diffusion coefficient at the peak energy from surrounding energies is significantly enhanced with frequency. When the increase is sharp enough, the precipitation of the particles with the highest diffusion coefficients can drastically reduce the flux and a trough can form in the middle of the spectrum. In Figure 4b, no REP flux is produced above ∼4 MeV since the diffusion coefficients in the loss cone are zero (Figure 1d).

[14] In Figure 5, we show the variation of the spectra of REP at 30 min for the full range of parameters. In the first few seconds (not shown), similar to the case of an initial distribution uniform in energy, with decreasing B_0 or increasing N_0, ω_1, or ω_2, J_{REP} increases at low energies but decreases at high energies. But at 30 min, in the case of lower B_0 or higher N_0, ω_1, or ω_2, the REP flux curves become fairly flat or doubly peaked, and sometimes intersect and fall below the curves of higher B_0 or lower N_0, ω_1, or ω_2 (e.g., the

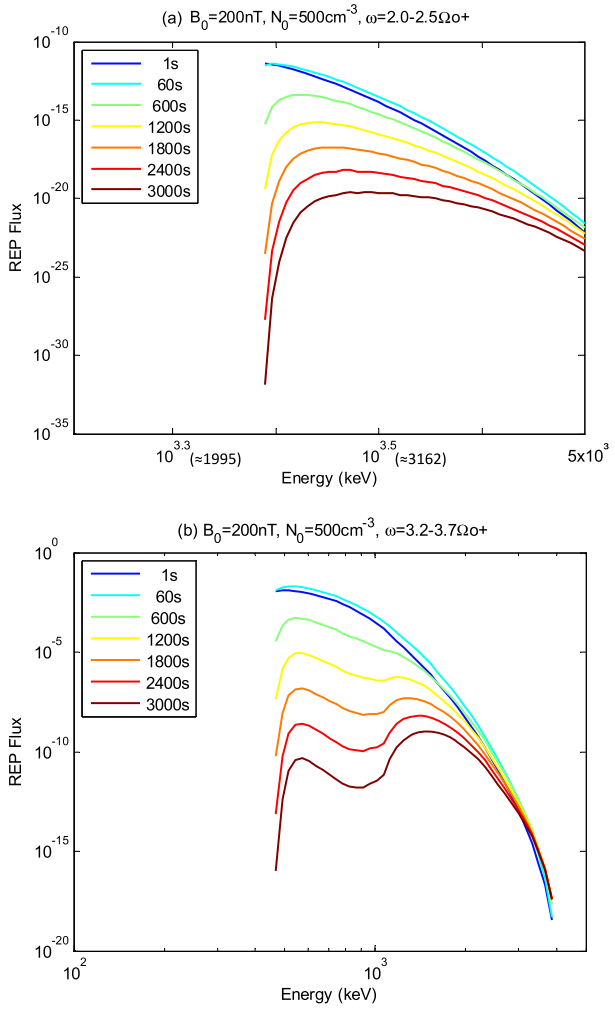

Figure 4. The energy distribution of the precipitating electrons at time 1 s to 50 min and the time evolution of the energies of the REP peaks assuming Maxwellian initial distribution equation (3). (a and b) B_0, N_0, ω_1, and ω_2 are the same as Figures 1c and 1d, respectively. Note the x axis left end in Figure 4a is higher than 100 keV for better visualization.

precipitation with B_0 = 125 nT is lower than that of 175 nT at ~2.6 MeV in Figure 5a; the precipitation with ω = 3.4-3.9 Ω_{O+} is lower than any other precipitation curve of ω_2 = 3.9 Ω_{O+} at below ~1 MeV in Figure 5c). When this happens, the role played by the changing parameter at these energy ranges is different than at early times. Our simulation also shows that increasing N_0, ω or decreasing B_0 lowers the energies of the peaks in both single- or double-peak spectra.

[15] In Figure 6, we integrate J_{REP} in the energy ranges 0.1–0.3, 0.3–1, and 1–5 MeV and vary two of the three parameters B_0, N_0, and ω simultaneously. These spectra can be compared with satellites with similar energy channels (e.g., POES and SAMPEX) [*Yando et al.*, 2011]. From high to low energy panels, the curves of the same color (for the same fixed parameter) get shorter and shorter, and can completely disappear when the energy of the channel is below the minimum resonant energies. With an increase in N_0 or ω or a decrease in B_0, the REP flux increases, except occasionally at late times when the roles played by the parameters reverse (explained in the previous paragraph), in which case strong initial scattering results in the significant decrease of the precipitation as the loss cone is depleted.

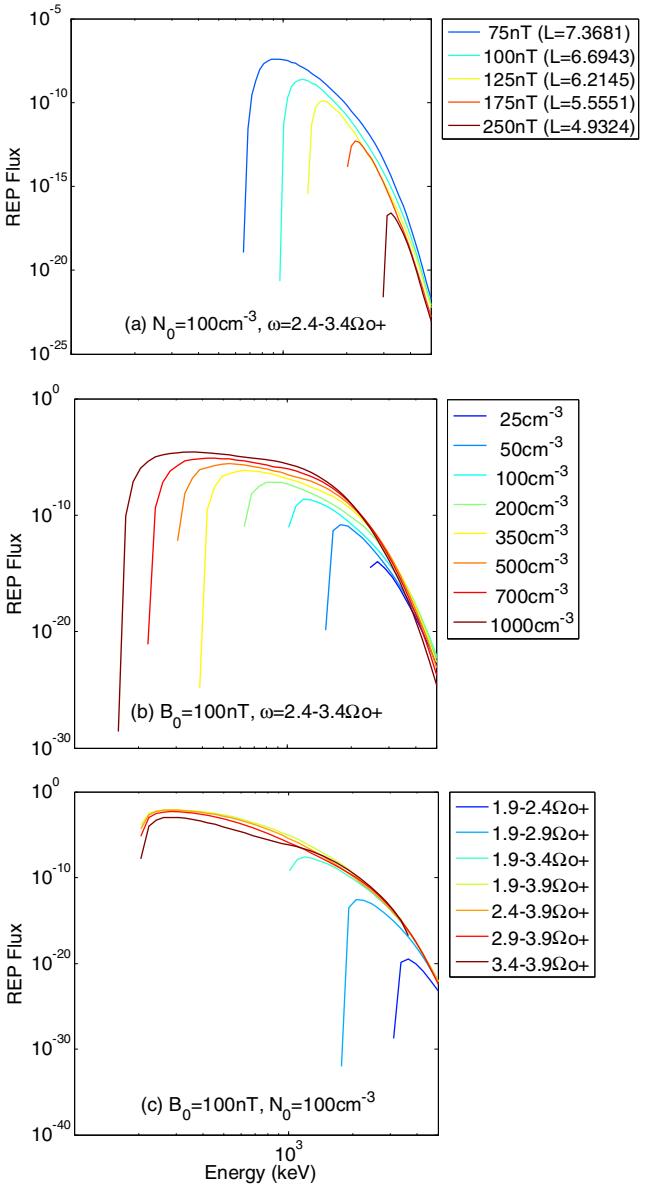

Figure 5. Energy spectra of precipitating electron flux at t = 30 min with Maxwellian initial distribution, plotted with the same parameters and color codes adopted in Figure 2. (c) The REP flux of 3.4–3.9 Ω_{O+} is zero above ~3.6 MeV where diffusion coefficients are zero in the loss cone.

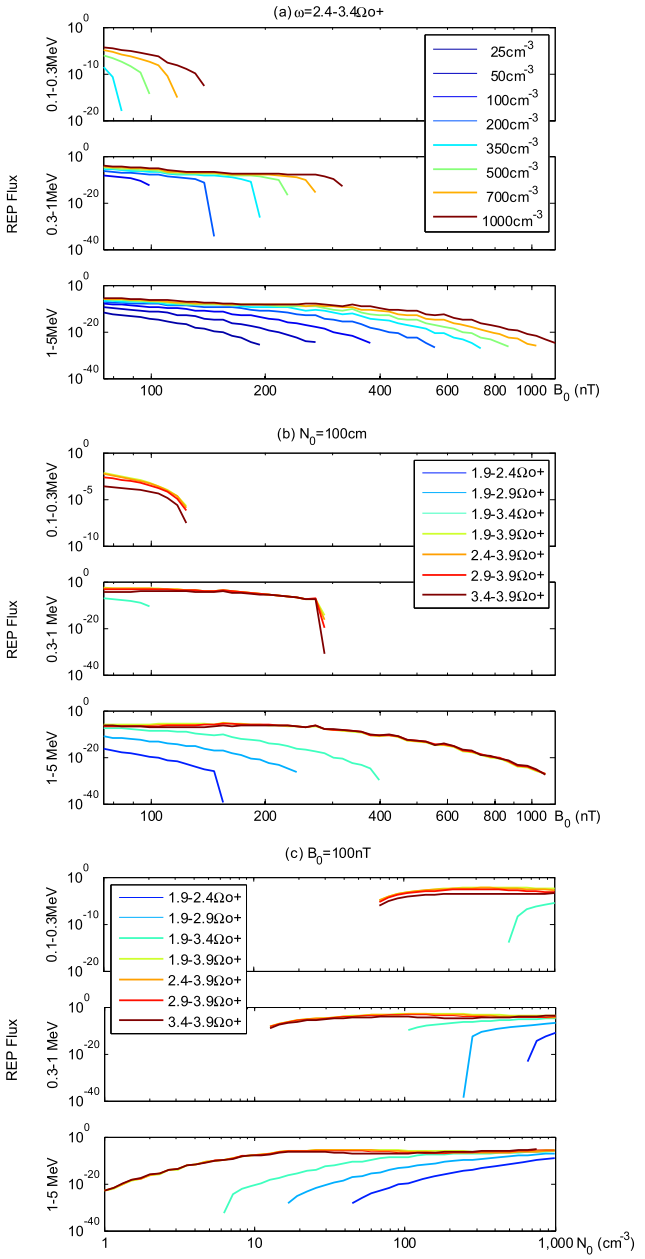

Figure 6. Precipitating electron flux in energy channels 0.1–0.3, 0.3–1, and 1–5 MeV at t = 30 min. (a) ω_1 = 2.4 Ω_{O+}, ω_2 = 3.4 Ω_{O+}, B_0 = 75–1150 nT, color-coded in N_0 ranging from 25 to 1000 cm^{-3}. (b) N_0 = 100 cm^{-3}, B_0 = 75–1150 nT, color-coded in ω ranging from 1.9–3.9 Ω_{O+}. (c) B_0 = 100 nT, N_0 = 1–1000 cm^{-3}, color-coded in ω ranging from 1.9 to 3.9 Ω_{O+}.

5. Summary and Discussion

[16] The goal of this paper is to investigate the shape of the energy spectrum of relativistic electron precipitation (REP) due to quasi-linear interactions with EMIC waves, and how it varies with time and changing parameters such as background magnetic field strength B_0, cold plasma density N_0, and wave frequency ω. The key results can be summarized as follows:

[17] 1. The REP energy spectrum is generally peaked, with a lower cutoff at the minimum resonant energy. Over time, the peak moves toward higher energies and the spectrum flattens (gets harder).

[18] 2. Increasing wave frequency can lead to the occurrence of a second peak. The first peak stays at a roughly constant energy. The second peak appears later at a higher energy and moves toward even higher energies.

[19] 3. In both single- and double-peak cases, the precipitating flux first rapidly increases as the loss cone is being filled, and then slowly decreases as the loss cone is being depleted.

[20] 4. Increasing N_0, ω, or decreasing B_0 lowers the minimum resonant energy and the energies of the peak(s). It causes the precipitation to increase at low energies and decrease at high energies. Over time, when strong scattering slows down, the role played by the changing parameter is altered.

[21] 5. The precipitation flux integrated over certain energy ranges can be compared with satellite measurements. We study how it is affected by changing parameters through varying two parameters at the same time. The integrated flux monotonically increases with increasing N_0 and ω and decreases with increasing B_0, except at the energies where the role of the parameter reverses when strong scattering causes a large reduction of the particles interacting with the waves (Figure 6).

[22] To better explain the variation of the precipitation energy spectrum, we show how the spectrum is affected by three deterministic factors—the diffusion coefficient, the initial trapped flux, and time.

[23] The diffusion coefficient is determined by the gyroresonance condition, the wave dispersion relation, and the wave frequency distribution and is a function of pitch angle. We calculate the diffusion coefficient for a range of input parameters B_0, N_0, and ω and characterize the pitch angle dependence of the diffusion coefficient with $\langle D_{\alpha\alpha}(\alpha_0 \sim 0^\circ, E)\rangle$, the upper pitch angle limit α_{0u}, and the maximum diffusion coefficient $\langle D_{\alpha\alpha}(\alpha_0, E)\rangle_m$ along with its corresponding pitch angle α_{0m}. We show that the diffusion coefficient maximizes at increasing pitch angles with increasing energy and the upper limit α_{0u} also increases. We also show that low B_0, high N_0 and high ω lower the minimum resonant energy, increase the diffusion coefficients of low energy particles and reduce the diffusion coefficients of high energy particles, and further increase the precipitation at low energies and decrease the precipitation at high energies at the beginning.

[24] The number of particles scattered into the loss cone per unit of time increases with the number of initially trapped particles. Therefore, when we switch the initial trapped flux energy distribution from uniform to Maxwellian, the spectrum becomes slanted with an enhancement at the lower energies, and the peak of the spectrum shifts to the left.

[25] The shape of the energy spectrum evolves as time goes on. Low pitch angle particles are scattered into the loss cone first. Therefore, in the beginning, the precipitation is strongly affected by the diffusion coefficients at low pitch angles. High pitch angle particles are scattered into the loss cone next. Since the diffusion coefficients tend to extend out and maximize at higher pitch angles with increasing energy, the precipitating flux of high energies has a growing relative significance over time, and the precipitation energy spectrum gets harder. In addition, if the scattering at a certain energy is initially strong, the particles at that energy are quickly lost and the precipitation will be largely reduced over time, and this also results in the rapid decrease of the precipitation at lower energies and the formation of the trough regions in the doubly peaked spectra.

[26] It is worth noting that thermal heating [*Anderson and Fuselier*, 1994; *Thorne et al.*, 2006] and the high plasma beta in the outer edge of the ring current during storm times [*Lui et al.*, 1987] may render the cold dispersion relation impractical. Several studies [*Isenberg*, 1984; *Chen et al.*, 2011; *Silin et al.*, 2011; *Chen et al.*, 2013] in which the hot dispersion relation is adopted suggest that at the vicinity of the ion cyclotron frequencies, the finite-beta effect may lead to the damping of the EMIC waves and the increase of the minimum resonant energies of relativistic electron scattering. Based on their conclusions, in the situations where the warm/hot ions are abundant, we should expect to see a higher minimum resonant energy cutoff in our REP energy spectrum if the wave frequencies are just below the helium gyrofrequency. Whether the doubly peaked spectra will still exist is uncertain because in our simulations, they usually only happen at high frequencies close to the helium gyrofrequency where the diffusion coefficient is significantly modified by the finite-beta effect.

[27] These model energy spectra show what we should expect to observe given various wave and geomagnetic environmental conditions if the precipitation is caused by EMIC wave scattering and can be simulated by the adopted diffusion model. Further work will include event studies in which we will take the input data from satellites (e.g., Van Allen Probes and GOES) and compare the simulated precipitating flux spectra with those detected by conjugate balloons (e.g., BARREL) and low altitude satellites (e.g., SAMPEX and POES).

[28] **Acknowledgments.** This work was supported at Dartmouth by NASA grant NNX08AM58G. We thank Richard E. Denton and Brian T. Kress from the Physics Department at Dartmouth for many useful discussions, Alex H. Barnett from the Math Department at Dartmouth for suggestions on numerical computation, Lunjin Chen, Jacob Bortnik, and Yuri Y. Shprits from UCLA, Jay M. Albert from Air Force Research Laboratory, Aleksandr Y. Ukhorskiy from Johns Hopkins University Applied Physics Laboratory, and Michael Schulz from Lockheed Martin Retiree for helpful comments.

[29] Robert Lysak thanks the reviewers for their assistance in evaluating this paper.

References

Albert, J. M. (2003), Evaluation of quasi-linear diffusion coefficients for EMIC waves in a multispecies plasma, *J. Geophys. Res.*, *108*(A6), 1–9, doi:10.1029/2002JA009792.

Albert, J. M. (2007), Simple approximations of quasi-linear diffusion coefficients, *J. Geophys. Res.*, *112*, A12202, doi:10.1029/2007JA012551.

Albert, J. M., and J. Bortnik (2009), Nonlinear interaction of radiation belt electrons with electromagnetic ion cyclotron waves, *Geophys. Res. Lett.*, *36*, L12110, doi:10.1029/2009GL038904.

Anderson, B. J., and D. C. Hamilton (1993), Electromagnetic ion cyclotron waves stimulated by modest magnetospheric compressions, *J. Geophys. Res.*, *98*(A7), 11,369–11,382, doi:10.1029/93JA00605.

Anderson, B. J., R. E. Erlandson, and L. J. Zanetti (1992a), A statistical study of Pc 1–2 magnetic pulsations in the equatorial magnetosphere: 2. Wave properties, *J. Geophys. Res.*, *97*(A3), 3089, doi:10.1029/91JA02697.

Anderson, B. J., R. E. Erlandson, and L. J. Zanetti (1992b), A statistical study of Pc 1–2 magnetic pulsations in the equatorial magnetosphere: 1. Equatorial occurrence distributions, *J. Geophys. Res.*, *97*(A3), 3075, doi:10.1029/91JA02706.

Anderson, B. J., and S. A. Fuselier (1994), Response of thermal ions to electromagnetic ion cyclotron waves, *J. Geophys. Res.*, *99*(A10), 19,413–19,425, doi:10.1029/94JA01235.

Bortnik, J., R. M. Thorne, T. P. O'Brien, J. C. Green, R. J. Strangeway, Y. Y. Shprits, and D. N. Baker (2006), Observation of two distinct, rapid loss mechanisms during the 20 November 2003 radiation belt dropout event, *J. Geophys. Res.*, *111*, A12216, doi:10.1029/2006JA011802.

Chen, L., R. M. Thorne, and R. B. Horne (2009), Simulation of EMIC wave excitation in a model magnetosphere including structured high-density plumes, *J. Geophys. Res.*, *114*, 1–11, doi:10.1029/2009JA014204.

Chen, L., R. M. Thorne, and J. Bortnik (2011), The controlling effect of ion temperature on EMIC wave excitation and scattering, *Geophys. Res. Lett.*, *38*, L16109, doi:10.1029/2011GL048653.

Chen, L., R. M. Thorne, Y. Shprits, and B. Ni (2013), An improved dispersion relation for parallel propagating electromagnetic waves in warm plasmas: Application to electron scattering, *J. Geophys. Res. Space Physics*, *118*, 2185–2195, doi:10.1002/jgra.50260.

Cornwall, J. M., F. V. Coroniti, and R. M. Thorne (1970), Turbulent loss of ring current protons, *J. Geophys. Res.*, *75*(25), 4699, doi:10.1029/JA075i025p04699.

Davidson, G., and M. Walt (1977), Loss cone distributions of radiation belt electrons, *J. Geophys. Res.*, *82*(1), 48, doi:10.1029/JA082i001p00048.

Erlandson, R. E., and A. J. Ukhorskiy (2001), Observations of electromagnetic ion cyclotron waves during geomagnetic storms: Wave occurrence and pitch angle scattering, *J. Geophys. Res.*, *106*(A3), 3883–3895, doi:10.1029/2000JA000083.

Foat, J. E., R. P. Lin, D. M. Smith, F. Fenrich, R. Millan, I. Roth, K. R. Lorentzen, M. P. McCarthy, G. K. Parks, and J. P. Treilhou (1998), First detection of a terrestrial MeV X-ray burst, *Geophys. Res. Lett.*, *25*(22), 4109, doi:10.1029/1998GL900134.

Fraser, B. J., H. J. Singer, W. J. Hughes, J. R. Wygant, R. R. Anderson, and Y. D. Hu (1996), CRRES Poynting vector observations of electromagnetic ion cyclotron waves near the plasmapause, *J. Geophys. Res.*, *101*(A7), 15,331, doi:10.1029/95JA03480.

Fraser, B. J., T. M. Loto'aniu, and H. J. Singer (2006), Electromagnetic ion cyclotron waves in the magnetosphere, in *Magnetospheric ULF Waves: Synthesis and New Directions, Geophys. Monogr. Ser.,* vol. 169, edited by K. Takahashi et al., pp. 195–212, AGU, Washington, D. C., doi:10.1029/GM16913.

Halford, A. J., B. J. Fraser, and S. K. Morley (2010), EMIC wave activity during geomagnetic storm and nonstorm periods: CRRES results, *J. Geophys. Res.*, *115*(A12), A12248, doi:10.1029/2010JA015716.

Horne, R. B., and R. M. Thorne (1993), On the preferred source location for the convective amplification of ion cyclotron waves, *J. Geophys. Res.*, *98*(A6), 9233, doi:10.1029/92JA02972.

Hu, Y., R. E. Denton, and J. R. Johnson (2010), Two-dimensional hybrid code simulation of electromagnetic ion cyclotron waves of multi-ion plasmas in a dipole magnetic field, *J. Geophys. Res.*, *115*, A09218, doi:10.1029/2009JA015158.

Isenberg, P. A. (1984), The ion cyclotron dispersion relation in a proton-alpha solar wind, *J. Geophys. Res.*, *89*(A4), 2133–2141, doi:10.1029/JA089iA04p02133.

Jordanova, V. K., C. J. Farrugia, R. M. Thorne, G. V. Khazanov, G. D. Reeves, and M. F. Thomsen (2001), Modeling ring current proton precipitation by electromagnetic ion cyclotron waves during the May 14–16, 1997, storm, *J. Geophys. Res.*, *106*, 7–22, doi:10.1029/2000JA002008.

Jordanova, V. K., J. Albert, and Y. Miyoshi (2008), Relativistic electron precipitation by EMIC waves from self-consistent global simulations, *J. Geophys. Res.*, *113*, A00A10, doi:10.1029/2008JA013239.

Kennel, C. F. (1966), Velocity space diffusion from weak plasma turbulence in a magnetic field, *Phys. Fluids*, *9*(12), 2377, doi:10.1063/1.1761629.

Kennel, C. F., and H. E. Petschek (1966), Limit on stably trapped particle fluxes, *J. Geophys. Res.*, *71*(1), 1, doi:10.1029/JZ071i001p00001.

Kokorowski, M., et al. (2008), Magnetospheric electric field variations caused by storm-time shock fronts, *Adv. Space Res.*, *42*(1), 181–191, doi:10.1016/j.asr.2008.03.006.

Li, W., Y. Y. Shprits, and R. M. Thorne (2007), Dynamic evolution of energetic outer zone electrons due to wave-particle interactions during storms, *J. Geophys. Res.*, *112*, 1–13, doi:10.1029/2007JA012368.

Lorentzen, K. R., M. P. McCarthy, G. K. Parks, J. E. Foat, R. M. Millan, D. M. Smith, R. P. Lin, and J. P. Treilhou (2000), Precipitation of relativistic electrons by interaction with electromagnetic ion cyclotron waves, *J. Geophys. Res.*, *105*(A3), 5381–5389, doi:10.1029/1999JA000283.

Lui, A. T. Y., R. W. McEntire, and S. M. Krimigis (1987), Evolution of the ring current during two geomagnetic storms, *J. Geophys. Res.*, *92*(A7), 7459–7470, doi:10.1029/JA092iA07p07459.

Lyons, L. R. (1973), Comments on pitch angle diffusion in the radiation belts, *J. Geophys. Res.*, *78*(28), 6793, doi:10.1029/JA078i028p06793.

Lyons, L. R., and D. Williams (1984), *Quantitative Aspects of Magnetospheric Physics*, pp. 240, Springer, Netherlands.

Meredith, N. P. (2003), Statistical analysis of relativistic electron energies for cyclotron resonance with EMIC waves observed on CRRES, *J. Geophys. Res.*, *108*(A6), 1–14, doi:10.1029/2002JA009700.

Millan, R., and R. Thorne (2007), Review of radiation belt relativistic electron losses, *J. Atmos. Sol. Terr. Phys.*, *69*(3), 362–377, doi:10.1016/j.jastp.2006.06.019.

Millan, R. M., R. P. Lin, D. M. Smith, K. R. Lorentzen, and M. P. McCarthy (2002), X-ray observations of MeV electron precipitation with a balloon-borne germanium spectrometer, *Geophys. Res. Lett.*, *29*(24), 2194, doi:10.1029/2002GL015922.

Millan, R. M., R. P. Lin, D. M. Smith, and M. P. McCarthy (2007), Observation of relativistic electron precipitation during a rapid decrease of trapped relativistic electron flux, *Geophys. Res. Lett.*, *34*, L10101, doi:10.1029/2006GL028653.

Millan, R. M., et al. (2013), The balloon array for RBSP relativistic electron losses (BARREL), *Space Sci. Rev.*, *179*, 503–530, doi:10.1007/s11214-013-9971-z.

O'Brien, T. P., M. Looper, and J. Blake (2004), Quantification of relativistic electron microburst losses during the GEM storms, *Geophys. Res. Lett.*, *31*, 2–5, doi:10.1029/2003GL018621.

Selesnick, R. S. (2006), Source and loss rates of radiation belt relativistic electrons during magnetic storms, *J. Geophys. Res.*, *111*, A04210, doi:10.1029/2005JA011473.

Shao, X., K. Papadopoulos, and A. S. Sharma (2009), Control of the energetic proton flux in the inner radiation belt by artificial means, *J. Geophys. Res.*, *114*, A07214, doi:10.1029/2009JA014066.

Shprits, Y. Y., L. Chen, and R. M. Thorne (2009), Simulations of pitch angle scattering of relativistic electrons with MLT-dependent diffusion coefficients, *J. Geophys. Res.*, *114*, A03219, doi:10.1029/2008JA013695.

Silin, I., I. R. Mann, R. D. Sydora, D. Summers, and R. L. Mace (2011), Warm plasma effects on electromagnetic ion cyclotron wave MeV electron interactions in the magnetosphere, *J. Geophys. Res.*, *116*, A05215, doi:10.1029/2010JA016398.

Summers, D. (2003), Relativistic electron pitch-angle scattering by electromagnetic ion cyclotron waves during geomagnetic storms, *J. Geophys. Res.*, *108*(A4), 1–12, doi:10.1029/2002JA009489.

Summers, D., B. Ni, and N. P. Meredith (2007), Timescales for radiation belt electron acceleration and loss due to resonant wave-particle interactions: 1. Theory, *J. Geophys. Res.*, *112*, A04206, doi:10.1029/2006JA011801.

Tao, X., J. M. Albert, and A. A. Chan (2009), Numerical modeling of multidimensional diffusion in the radiation belts using layer methods, *J. Geophys. Res.*, *114*, A02215, doi:10.1029/2008JA013826.

Thorne, R. M., and C. F. Kennel (1971), Relativistic electron precipitation during magnetic storm main phase, *J. Geophys. Res.*, *76*(19), 4446, doi:10.1029/JA076i019p04446.

Thorne, R. M., R. B. Horne, V. K. Jordanova, J. Bortnik, and S. Glauert (2006), Interaction of EMIC waves with thermal plasma and radiation belt particles, in *Magnetospheric ULF Waves: Synthesis and New Directions, Geophys. Monogr. Ser.,* vol. 169, edited by K. Takahashi et al., pp. 213–223, AGU, Washington, D. C., doi:10.1029/GM169.

Ukhorskiy, A. Y., Y. Y. Shprits, B. J. Anderson, K. Takahashi, and R. M. Thorne (2010), Rapid scattering of radiation belt electrons by storm-time EMIC waves, *Geophys. Res. Lett.*, *37*, L09101, doi:10.1029/2010GL042906.

Usanova, M. E., I. R. Mann, J. Bortnik, L. Shao, and V. Angelopoulos (2012), THEMIS observations of electromagnetic ion cyclotron wave occurrence: Dependence on AE, SYMH, and solar wind dynamic pressure, *J. Geophys. Res.*, *117*, A10218, doi:10.1029/2012JA018049.

Yando, K., R. M. Millan, J. C. Green, and D. S. Evans (2011), A Monte Carlo simulation of the NOAA POES medium energy proton and electron detector instrument, *J. Geophys. Res.*, *116*, A10231, doi:10.1029/2011JA016671.